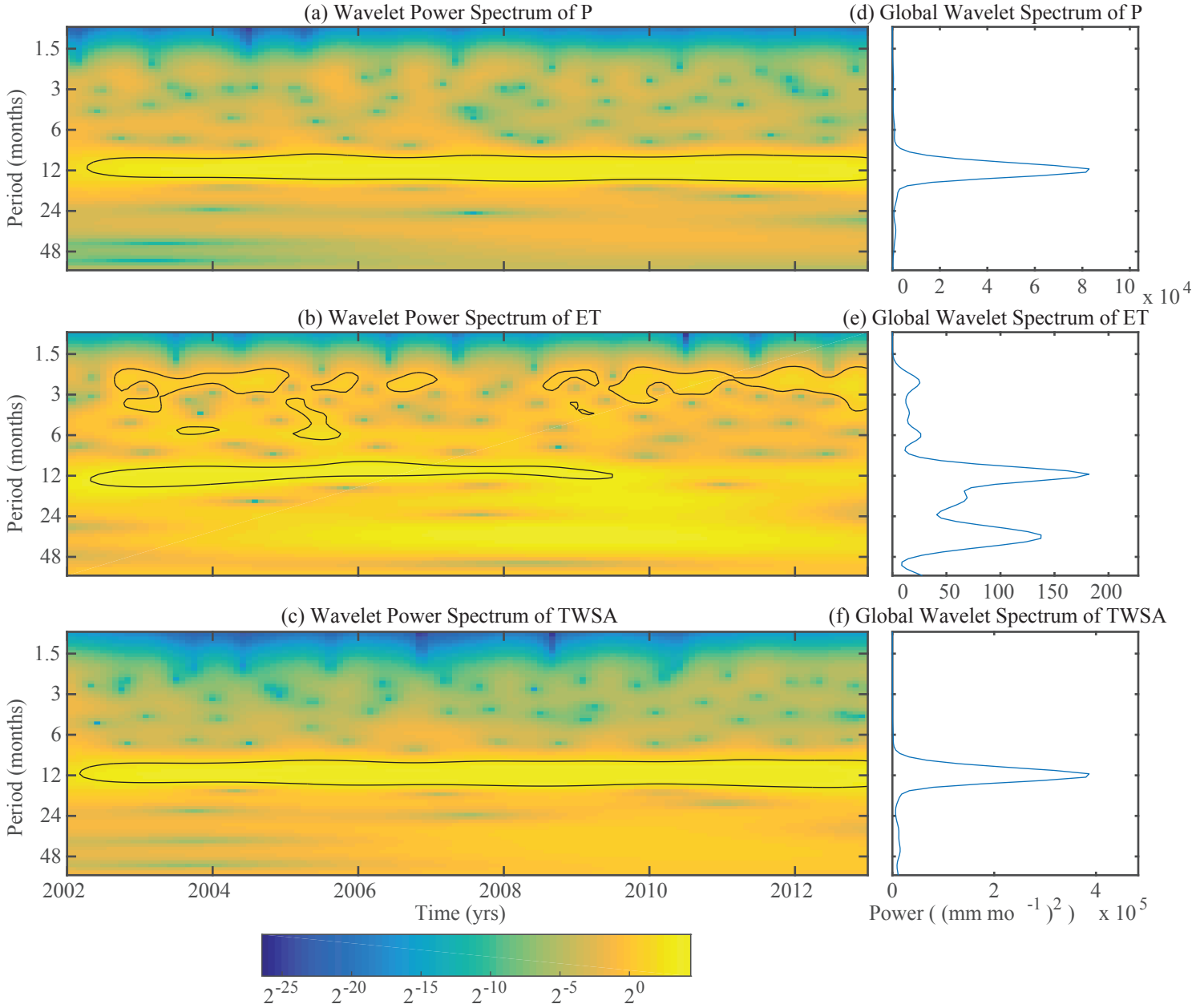

Figure 1. Contour plots of wavelet power spectra of precipitation (a), ET (b), and TWSA (c), and global wavelet spectra of precipitation (d), ET (e) and TWSA (f). The x-axes of subplots (a), (b), and (c) represent the time, the y-axis represents the periodicity scale, and the color represents the magnitude of the wavelet coefficient. The contour lines enclose regions of greater than 95% confidence (Torrence and Compo 1998). The x-axes of subplots (d), (e), and (f) represent the power of global wavelet spectrum.

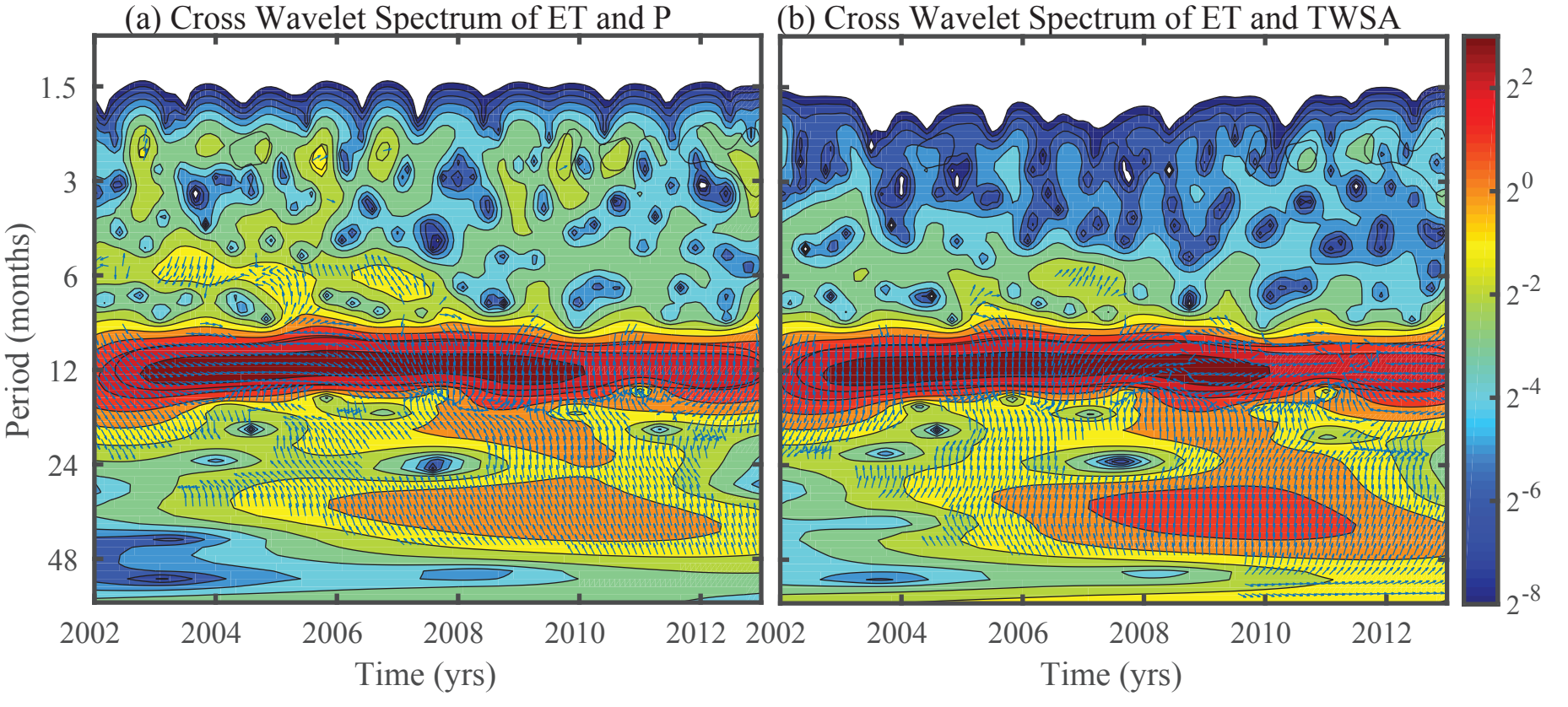

Figure 2. Cross wavelet power spectra of ET and P (a), and ET and TWSA (b). The contour plots represent the power of cross spectra and are shown as blank when the values are smaller than 2-8. The arrows represent the phase relationship between these time series and are only presented when the wavelet power is greater than 2^{-2}.

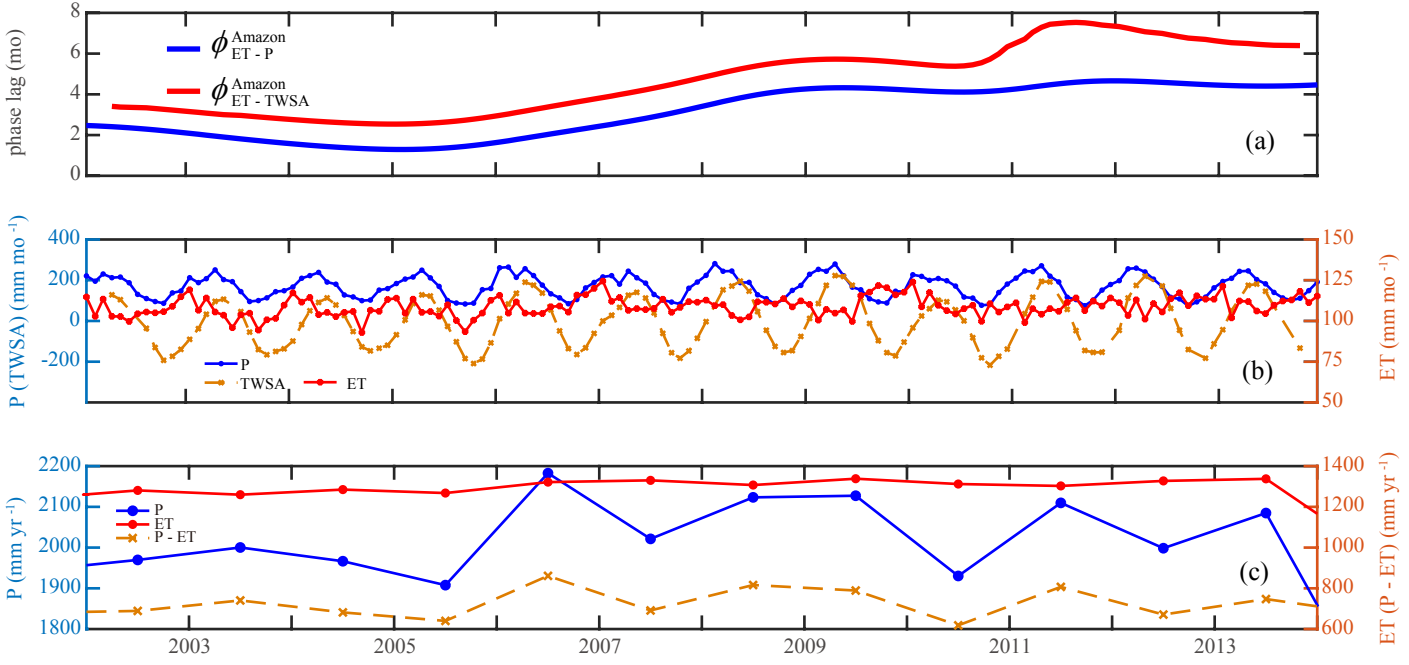

Figure 3. Plots of phase lags (a) between ET and P ($\phi^{\text{Amazon}}_{\text{ET - P}}$), and between ET and TWSA ($\phi^{\text{Amazon}}_{\text{ET - TWSA}}$); monthly time series data (b) of P, TWSA, and ET; and annual averaged data (c) of P, ET, and P – ET. All time series data are spatially-averaged over the Amazon, and the phase lags are calculated based on the spatially-averaged monthly time series data.

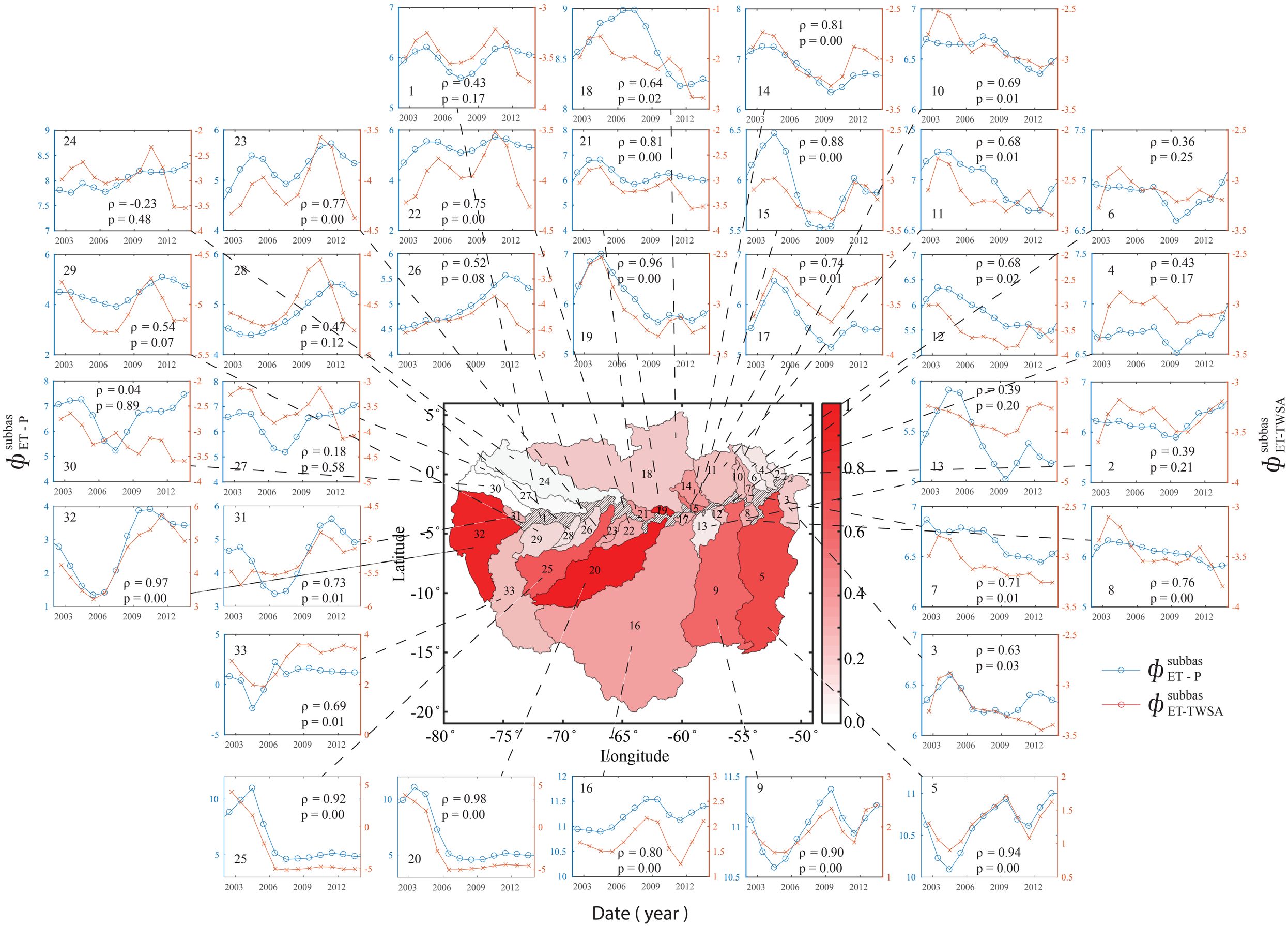

Figure 4. Sub-basins of Amazon (center subplot) and the phase lags between ET and P ($\phi^{\text{subbas}}_{\text{ET-P}}$), and between ET and TWSA ($\phi^{\text{subbas}}_{\text{ET-TWSA}}$) (subplots 1 – 33). The color saturation in the center sub-plot indicates the linear correlation coefficients between $\phi^{\text{subbas}}_{\text{ET-P}}$ and $\phi^{\text{subbas}}_{\text{ET-TWSA}}$. Darker means higher correlation as shown in the legend. The location of subplots 1 – 33 are generally corresponding to the geographical position as shown in the center subplot. Subplots 1 – 33 also show the linear correlation coefficients and p-values for testing the hypothesis of no correlation against the alternative that there is a nonzero correlation. If p is small (i.e., $p < 0.05$), then the correlation is significantly different from zero. The x-axes of subplots 1 – 33 are the time (year), the left y-axes of them are $\phi^{\text{subbas}}_{\text{ET-P}}$ and the right ones are $\phi^{\text{subbas}}_{\text{ET-TWSA}}$

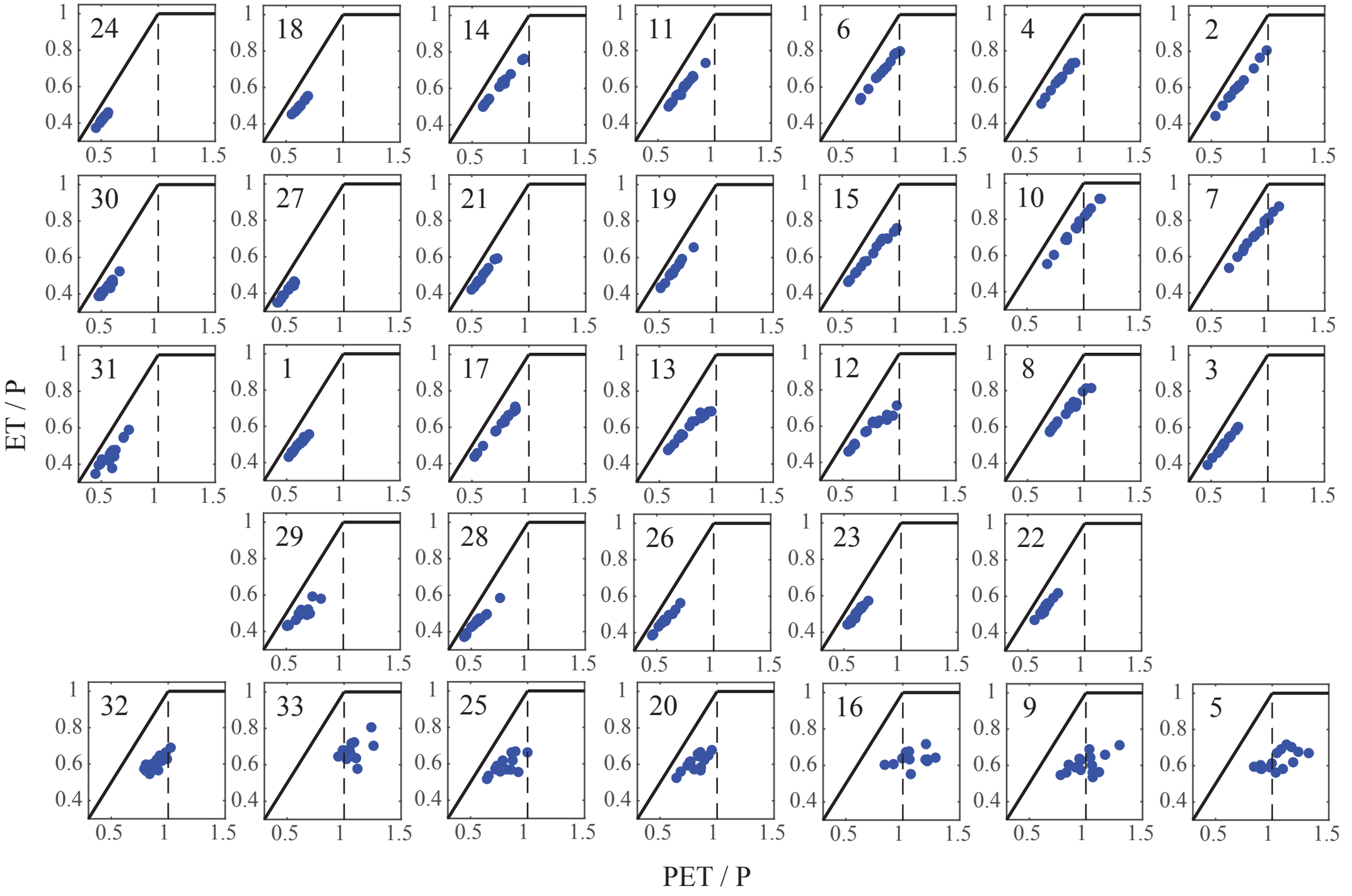

Figure 5. The Budyko framework applied to 33 sub-basins of Amazon. In each subplot, the x-axes are the ratio between potential evapotranspiration and precipitation (PET / P); the y-axes are the ratio between actual ET and precipitation (ET / P); the solid horizontal line indicates water limitation (i.e., annual ET = annual P); the 1:1 line indicates energy limitation (annual ET = annual PET); the dashed vertical line indicates the boundary between these limitations; and the dots are the annual averaged data for each sub-basin. The label of each subplot corresponds to the index of each sub-basin (see Fig. 7) and the positions of them are generally corresponding to the geographical location of each sub-basin.

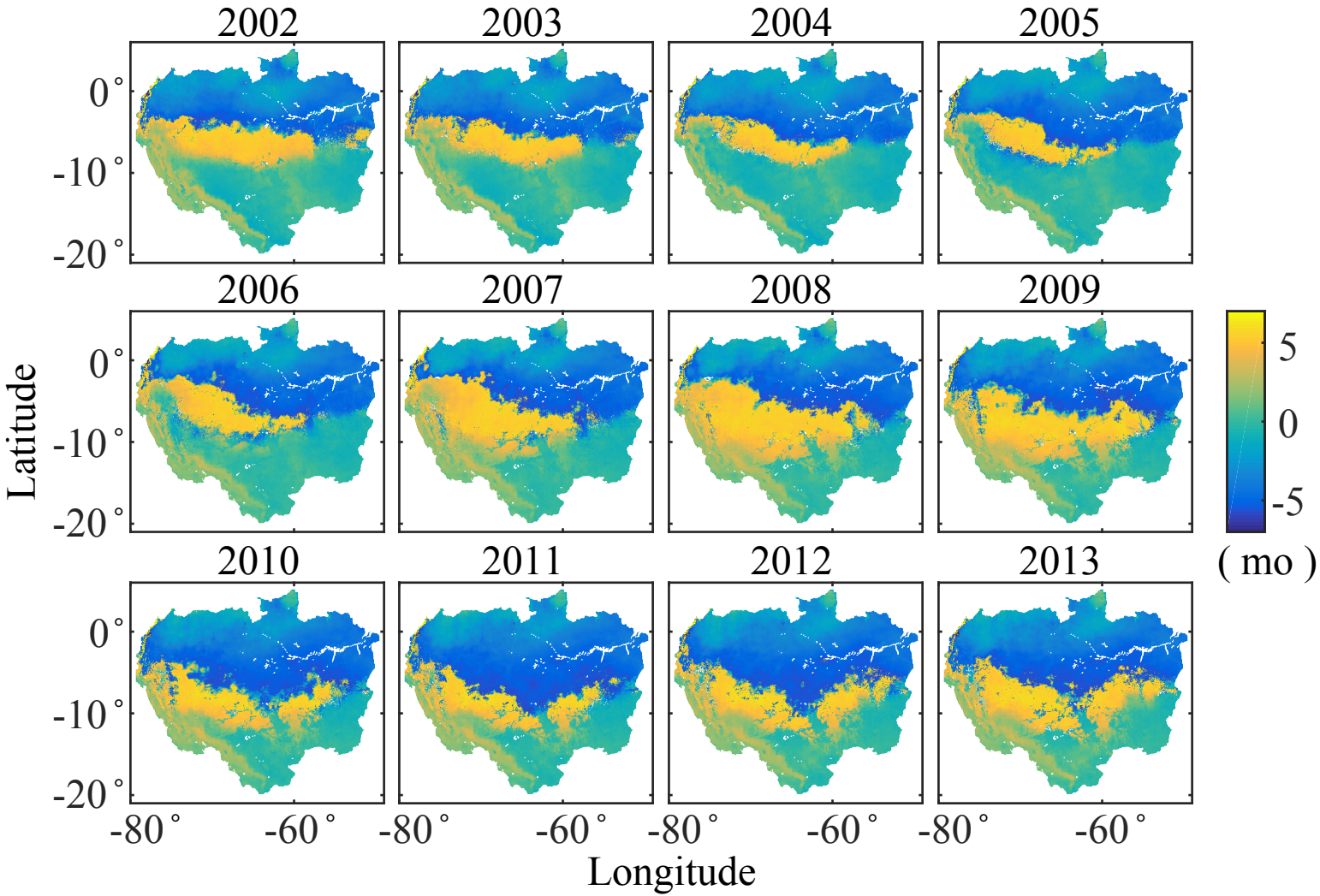

Figure 6. Map of the pixel-by-pixel phase lag between ET and P ($\phi_{\text{ET-P}}^{1\text{ km}}$) for each year from 2002 to 2013. Different colors represent different phase lags in time (month) as shown in the legend. Missing data from either ET or P are shown as blank.

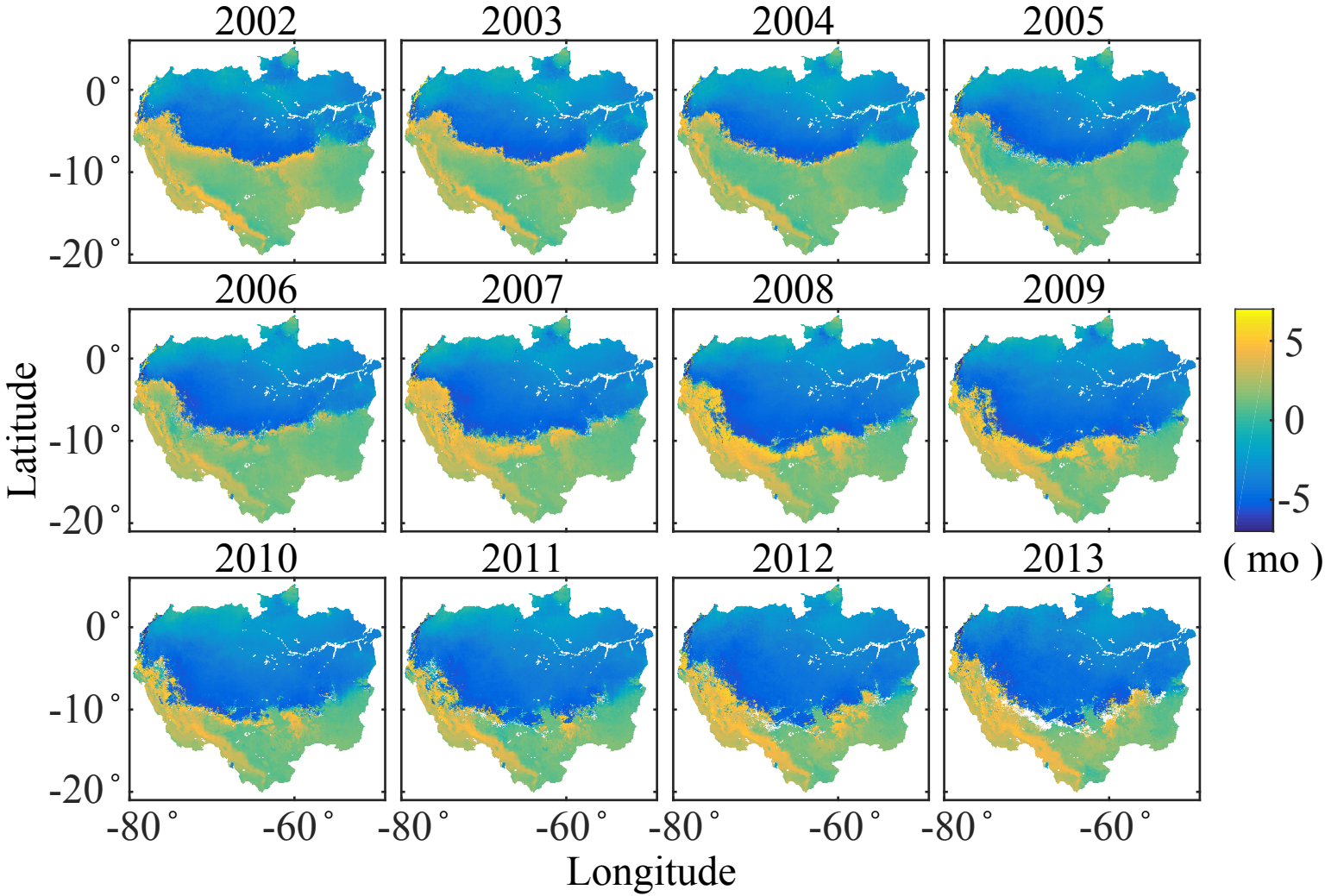

Figure 7. Map of the pixel-by-pixel phase lag between ET and TWSA ($\phi^{1\,km}_{ET\text{-}TWSA}$) for each year from 2002 to 2013. Different colors represent different phase lags in time (month) as shown in the legend. Missing data from either ET or TWSA are shown as blank.

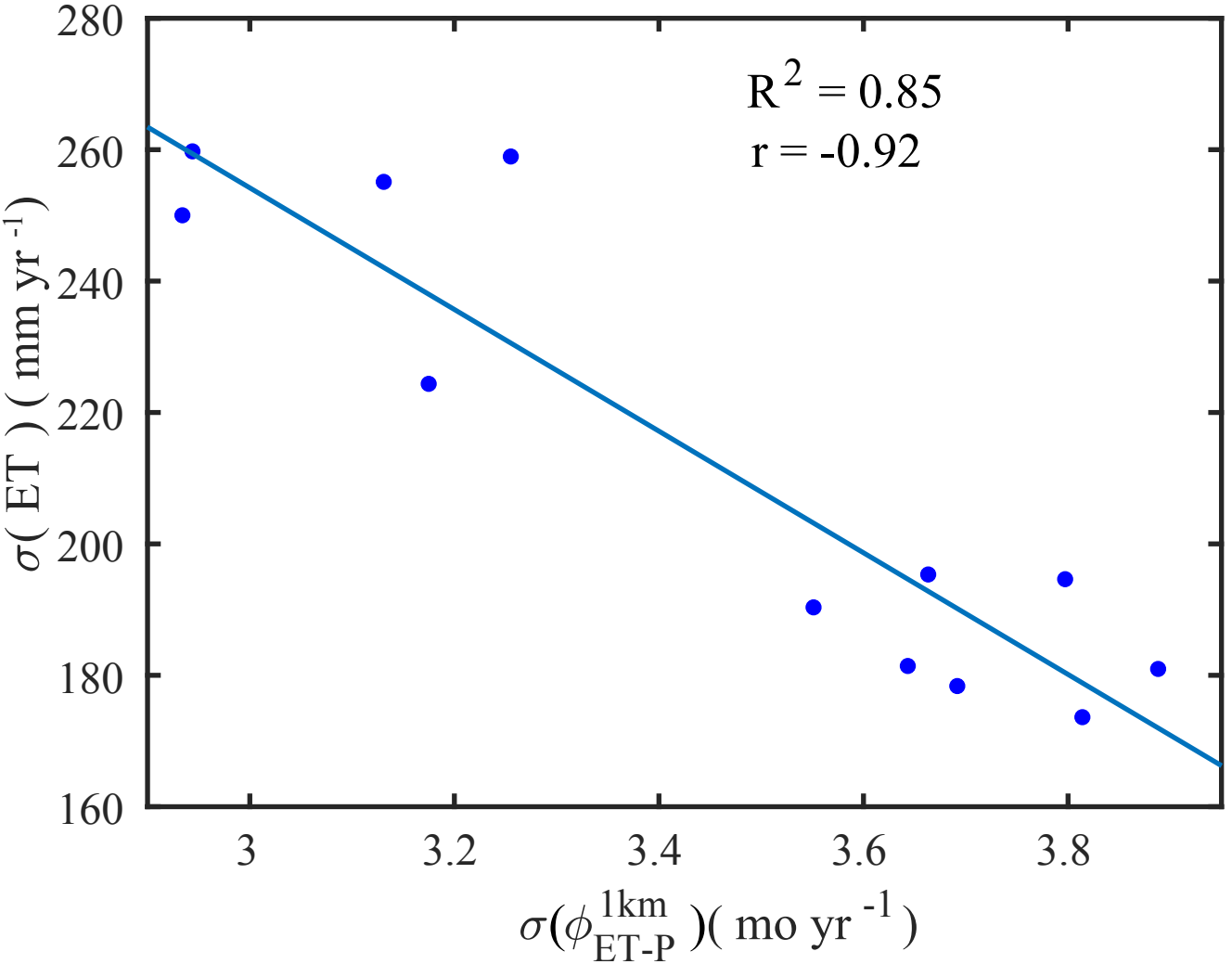

Figure 8. Correlation plot of the spatial standard deviation of the pixel-by-pixel annual averaged phase lag between ET and P ($\sigma\ \varphi_{ET-P}^{1\ km}$) and the standard deviation of annual averaged ET (σET). The dots are the data and the solid line is the fitting curve.

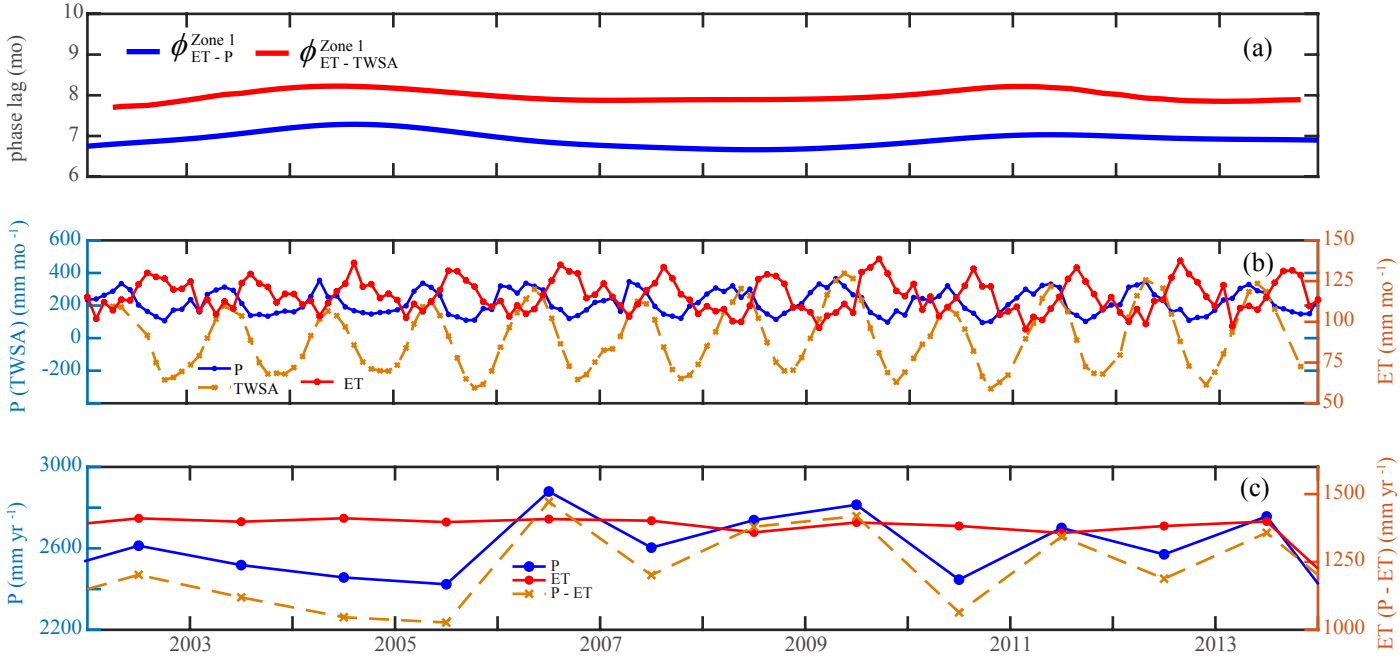

Figure 9. Plots of (a) phases between ET and P ($\phi^{\text{Zone 1}}_{\text{ET - P}}$), and between ET and TWSA ($\phi^{\text{Zone 1}}_{\text{ET - TWSA}}$); (b) monthly time series of P, TWSA, and ET; and (c) annual averages of P, ET, and P − ET. All time series data are spatially averaged over Zone 1, and the phases are calculated based on the spatially averaged monthly variables of Zone 1.

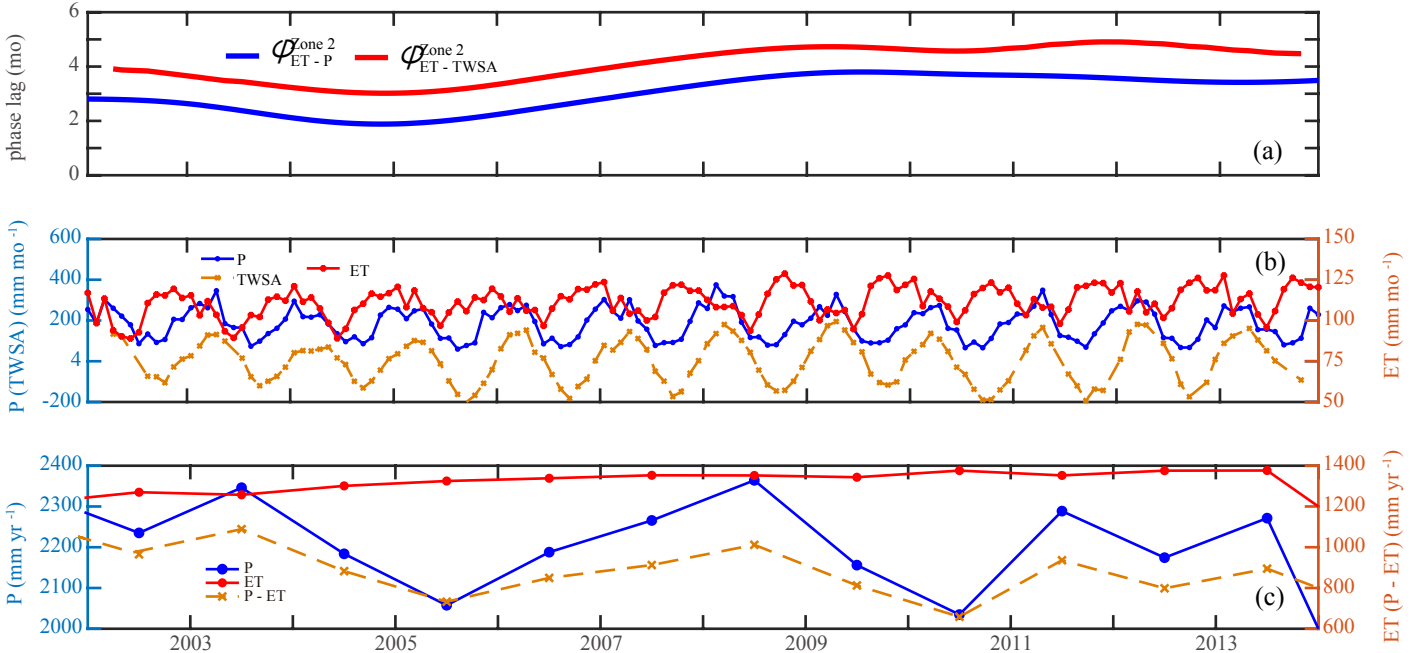

Figure 10. Plots of (a) phases between ET and P ($\varphi^{\text{Zone 2}}_{\text{ET - P}}$), and between ET and TWSA ($\varphi^{\text{Zone 2}}_{\text{ET - TWSA}}$); (b) monthly time series of P, TWSA, and ET; and (c) annual averages of P, ET, and P − ET. All time series data are spatially averaged over Zone 2, and the phases are calculated based on the spatially averaged monthly variables of Zone 2.

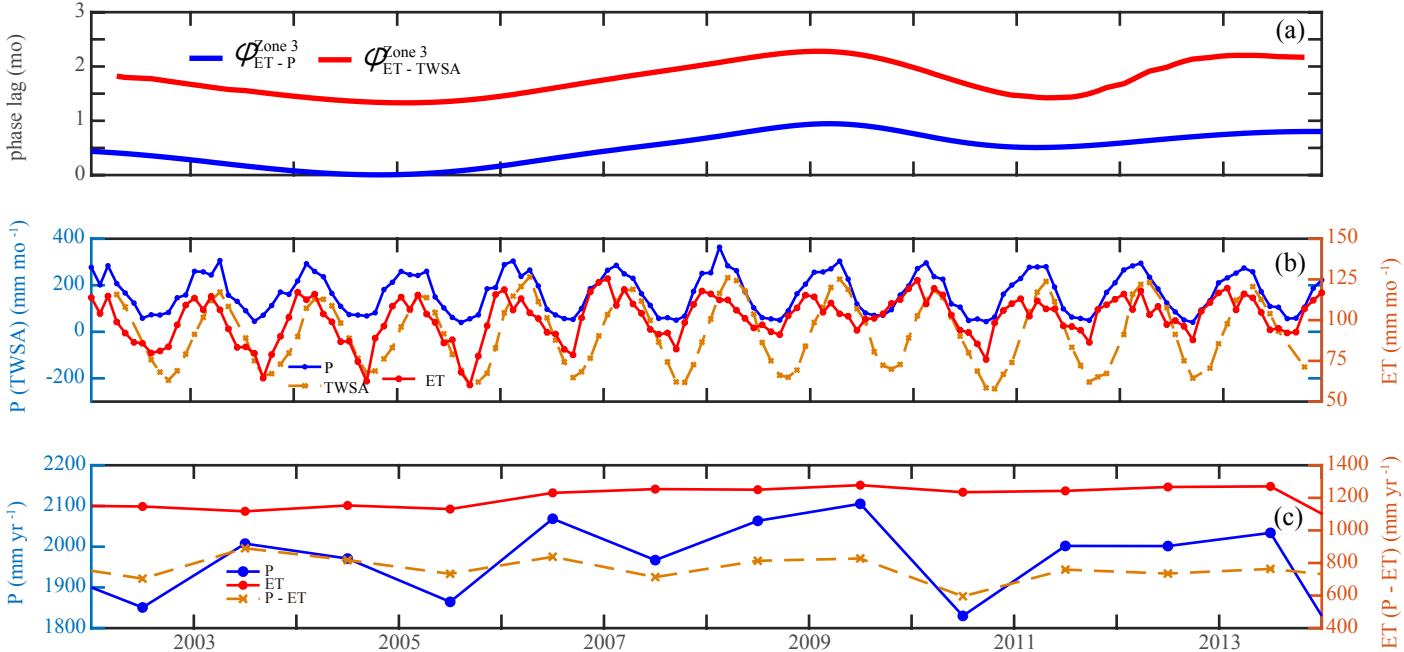

Figure 11. Plots of (a) phases between ET and P ($\varphi_{ET-P}^{Zone\ 3}$), and between ET and TWSA ($\varphi_{ET-TWSA}^{Zone\ 3}$); (b) monthly time series of P, TWSA, and ET; and (c) annual averages of P, ET, and P − ET. All time series data are spatially averaged over Zone 3, and the phases are calculated based on the spatially averaged monthly variables of Zone 3.